Postprint of: Sobczak Z., Winiarski M., Xie W., Cava R., Klimczuk T., Superconductivity in the intermetallic compound Zr_5Al_4, EPL-EUROPHYS LETT, Vol. 127, Iss. 3 (2019), 37005, DOI: 10.1209/0295-5075/127/37005

Superconductivity in the intermetallic compound Zr_5Al_4

Z. Sobczak[1,*], M.J. Winiarski[1], W. Xie[2], R. J. Cava[3], and T. Klimczuk[1,†]

[1]*Faculty of Applied Physics and Mathematics, Gdansk University of Technology, Narutowicza 11/12, 80-233 Gdansk, Poland*

[2]*Department of Chemistry, Louisiana State University, Baton Rouge, LA, USA 70803*
[3]*Department of Chemistry, Princeton University, Princeton New Jersey 08544, USA*

* zuzanna.sobczak@pg.edu.pl; † tomasz.klimczuk@pg.edu.pl

Abstract

Polycrystalline Zr_5Al_4 was synthesized using the arc-melting method. Powder X-ray diffraction confirms the previously reported crystal structure of the Ti_5Ga_4-type (*P6₃/mcm*) with lattice parameters: a = 8.4312(6) Å, and c = 5.7752(8) Å. Electrical resistivity and low temperature magnetic susceptibility studies indicate that Zr_5Al_4 exhibits superconducting behavior below 2 K. The normalized heat capacity jump at T_c = 1.82 K, $\Delta C/\gamma T_c$ = 1.41, confirms the bulk superconductivity. The Sommerfeld coefficient γ = 29.4 mJ mol^{-1} K^{-2} and the Debye temperature Θ_D = 347 K were obtained by fitting the low temperature heat capacity data. The electron-phonon coupling strength $\lambda_{el\text{-}ph}$ = 0.48 and estimated upper critical field $\mu_0 H_{c2}(0)$ = 1.09 T (dirty limit) suggest that Zr_5Al_4 is a weakly coupled type-II superconductor. First-principles calculations show the presence of a van Hove singularity near the Fermi Energy.

I Introduction

Superconductivity has been an interesting topic for study since its discovery in 1911 in mercury. Prediction of new superconducting materials remains challenging, with several approaches were invented until now. Looking for new superconductors within structural families known to host superconductors increases the odds for discovering new ones. One such structure-based superconducting system is based on Ga building blocks, where several superconductors have been found [1–6]. Due to its similarity to gallium, aluminum is a good candidate for expanding the search in this family. Superconductivity has been found in MT_2Al_{20} (M=Sc, Lu, Y, La, Pr; T = Ti, V, Nb, Ta) cage compounds, for example, likely driven by a rattling effect [7–10].

Endohedral cluster compounds are usually built of alkali or alkaline-earth metals that donate electrons to stabilize the structure. A less obvious candidate for creating cluster phases is Zr. Its electronegativity (χ = 1.33 in Pauling's scale [11]) places Zr in the vicinity of atoms that are usually referred to as structure-stabilizing due to electron donation such as Mg (χ = 1.31) or Na (χ = 0.93). Therefore, Zr in a Zr-Al bond is a weak electropositive donor of electrons (χ(Zr) = 1.33, χ(Al) = 1.61), and thus from the chemical point of view fulfills the requirements for forming an endohedral cluster.

Zr_5Al_4 was first reported as an additional phase in a Zr_3Al_2 sample [12]. It is a member of the Ti_5Ga_4-type family, with a crystal structure consisting of Al decahedra surrounding one site of Zr atoms, as shown in Fig. 1.

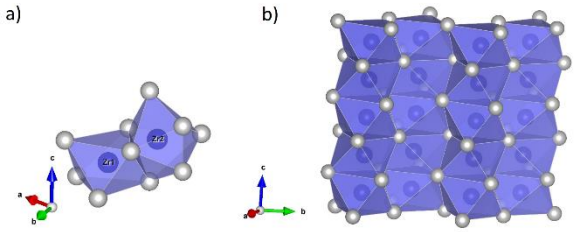

Fig. 1 Crystal structure of Zr_5Al_4.Zirconium and aluminum atoms are represented by blue and silver balls, respectively.1 a) Trigonal bipyramidal cluster of Al around Zr1 atom and double decahedral cluster of Al surrounding Zr2 atom b) Set of double decahedral clusters of Al atoms surrounding Zr1 atoms in unit cell. Image rendered using VESTA [40].

The $ZrAl_7$ cluster can be considered as a building block of the structure, similar to the case for Zr_2Al_3 where the cluster consists of 8 Al atoms [13,14]. Since obtaining pure Zr_5Al_4 is nontrivial, the physical properties have been unknown until now. Density functional theory (DFT) calculations of the electronic structure show the presence of a van Hove singularity around the Fermi level that may be important for the superconductivity in Zr_5Al_4. The metastable character of Zr_5Al_4 is reflected in the results of high throughput DFT calculations on the Zr-Al system, as the calculated total energy places the phase above the convex hull [15,16]. Here we report that this material is a type-II superconductor, describing its synthesis and electronic properties.

II Materials and Methods

A polycrystalline sample of Zr_5Al_4 was synthesized by arc-melting elemental zirconium (rod, 99.2%, Alfa Aesar) and aluminum (shot, 99.99%, Alfa Aesar) in the MAM-1 Edmund Buhler arc furnace on a water-cooled copper hearth with high purity argon (5N) atmosphere. After each melting a sample button was turned and re-melted four times to ensure homogeneity. Estimated mass loss was around 1% and was compensated by 2% excess of Al. The as-cast sample was used for the structural and physical studies.

The phase purity of a crushed sample at room temperature was evaluated using powder X-ray diffraction (PXRD) on the Bruker D2 Phaser 2nd generation diffractometer using Cu-Kα radiation and a LynxEye XE-T detector. The PXRD pattern was analyzed using a Pawley fit [17] with the Diffrac.SuiteTopas software [18].

All electronic property measurements were performed using a Quantum Design Dynacool Physical Property Measurement System (PPMS). For magnetic susceptibility studies, a vibrating sample magnetometer (VSM) technique was employed. Heat capacity characterization was performed on a polished sample using the standard 2τ relaxation method in the PPMS system equipped with ^{3}He cooling. Electrical resistivity measurements were performed on a sample with Pt (50 μm dia.) wires that were spark welded to a polished flat sample surface.

The band structures and Density of States (DOS) of Zr_5Al_4 were calculated using WIEN2k with local density approximation (LDA)-type pseudopotentials. The electronic structure calculations were performed with and without spin-orbit coupling (SOC). Reciprocal space integrations were completed over a 6×6×8 Monkhorst-Pack *k*-point mesh. The convergence criterion for self-consistent field calculation is 0.1meV.

III Results

A room temperature PXRD measurement was performed in order to confirm the phase purity of the Zr_5Al_4 sample. The result is presented in Fig. 2.

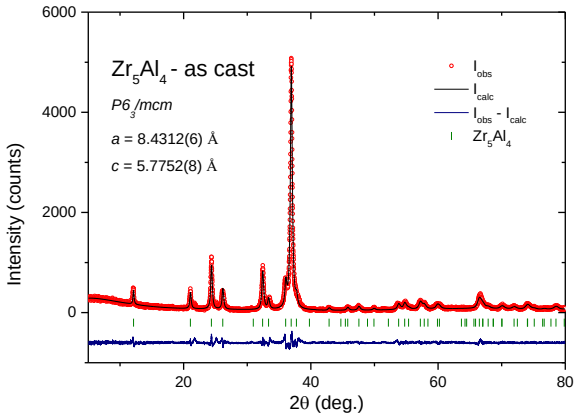

Fig. 2 The X-ray powder diffraction characterization of a crushed Zr_5Al_4 as-cast sample. The plot shows the Pawley fit (black solid line) to the measured intensity (red dots). The blue line shows the difference between measured and calculated intensity. Green ticks represent the expected positions of Bragg reflections for Zr_5Al_4 compound. Figures of merit are R_p(%) = 8.72, R_{wp}(%) = 11.81, R_{exp}(%) = 8.57, χ^2 = 1.38.

All the Bragg lines in the PXRD pattern are indexed with the hexagonal *P6$_3$/mcm* unit cell of Ti_5Ga_4-type material. The Pawley fit, represented by a black solid line in Fig. 2, gave the lattice parameters: *a* = 8.4312(6) Å and *c* = 5.7752(8) Å, which are in good agreement with the values reported previously [12].

The sample is stable in air and does not show any signs of decomposition after 14 days. The as-cast sample was found to be of the highest purity, did not contain any additional phases and was used for further evaluation. No heat treatment was used for further annealing of the sample, since according to the Zr-Al phase diagram [15], Zr_5Al_4 is a high temperature phase. Annealing and air or water quenching after annealing at temperatures of 1000°C – 1150°C did not result in obtaining a single Zr_5Al_4 compound. The observed instability of Zr_5Al_4 is in agreement with the results of the DFT-based total energy calculations available in the Materials Project database [19]. Zr_5Al_4 is 45 meV above the convex hull for the Zr-Al system [16] and is neighbored by two stable phases: Zr_4Al_3 and Zr_2Al_3 [20,21]. Those are the phases that form in our experiments upon annealing Zr_5Al_4.

To characterize the superconducting transition of Zr_5Al_4, zero-field cooled (ZFC) and field cooled (FC) dc volume susceptibility $\chi_V = M_V/H$ was measured in the temperature range of 1.68 – 2.4 K, with a magnetic field of H = 10 Oe. The results are shown in the main panel of Fig. 3.

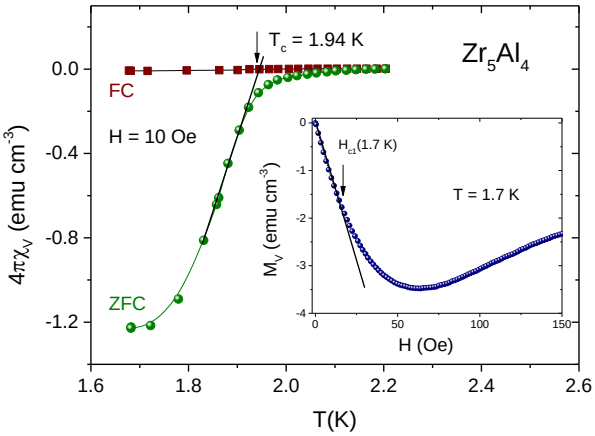

Fig. 3 Main Panel: The zero-field cooled (ZFC) and field cooled (FC) volume susceptibility $\chi_V(T)$ through the superconducting transition, measured in a field of 10 Oe. Inset: magnetization vs. magnetic field M(H) at T=1.7 K.

The superconducting transition temperature T_c = 1.94 K is defined as the temperature where the extrapolation of the steepest slope of $\chi(T)$ intersects the extrapolation of the normal state susceptibility to lower temperatures [22]. At the lowest temperature, χ_V starts to saturate and the magnetic susceptibility $4\pi\chi_V$ is -1.2. This stronger than expected ($4\pi\chi_V$ = -1) diamagnetic signal is due to the fact that we did not consider the demagnetization effect. The inset of Fig 3. presents magnetization vs. magnetic field M(H) collected at 1.7 K. The shape of M(H) curve suggests that Zr_5Al_4 is a type-II superconductor with a lower critical field at T=1.7 K equal to $\mu_0H_{c1}(1.7K)$ = 16 Oe. Magnetic measurements below 1.68 K are required for more detailed analysis in order to estimate the demagnetization factor (N) and the lower critical field $H_{c1}(0)$.

The temperature dependence of the heat capacity $C_p(T)$ measured at temperatures in the vicinity of the superconducting transition is presented in Fig. 4(a).

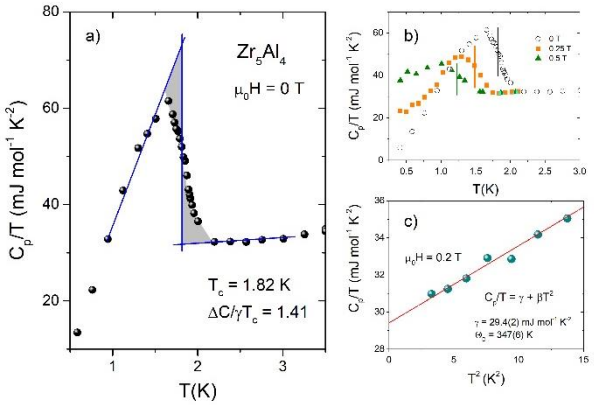

Fig. 4. Low temperature specific heat of Zr_5Al_4. (a) Superconducting anomaly under zero applied magnetic field. The size of the anomaly is estimated using the conserved entropy construction, (b) superconducting transition in different applied magnetic fields, (c) C_p/T vs, T^2 in the normal state region, measured in magnetic field of 0.2 T

The bulk nature of the superconductivity in Zr_5Al_4 is confirmed by a sharp anomaly seen at temperature T_c = 1.82 K, which is slightly lower than the T_c obtained from the magnetic susceptibility measurements. The value of the specific heat jump at T_c, estimated with the equal entropy construction method, is $\Delta C/T_c$ = 42.8 mJ mol^{-1} K^{-2}. Fig. 4(c) shows a plot of C_p/T versus T^2, measured in an applied field of 0.2 T. The solid line through the data points represents a fit by the expression $\frac{C_P}{T} = \gamma + \beta T^2$, where the first term is the normal state electronic contribution and latter one comes from the lattice specific heat. The fit gave the Sommerfeld coefficient γ = 29.4(2) mJ mol^{-1} K^{-2} and β = 0.42(2) mJ mol^{-1} K^{-4}. The Debye temperature is then calculated using the relation: $\Theta_D = \sqrt[3]{\frac{12\pi^4 nR}{5\beta}}$, (1)

where n is the number of atoms per formula unit (here n = 9) and R is the gas constant (R = 8.31 J mol^{-1} K^{-1}). The obtained value of the Debye temperature is Θ_D = 347(6) K. The resulting value is about 20% lower than the Debye temperature of Aluminum (Θ_D = 428 K [23]) and about 23% higher than the Debye temperature of Zirconium (Θ_D = 290 K [24]). Using previously obtained $\Delta C/T_c$ = 42.8 mJ mol^{-1} K^{-2} and γ = 29.4(2) mJ mol^{-1} K^{-2}, we got $\Delta C/\gamma T_c$= 1.41. This value is very close to the weak coupling superconductivity limit predicted by the BCS theory ($\Delta C/\gamma T_c$=1.43).

Knowing the Debye temperature and T_c, and taking the Coulomb pseudopotential parameter μ^* = 0.13 [25–27], the electron – phonon coupling can be estimated from the inverted McMillan formula [28]:

$$\lambda_{el-ph} = \frac{1.04+\mu^* \ln\left(\frac{\Theta_D}{1.45T_c}\right)}{(1-0.62\mu^*)\ln\left(\frac{\Theta_D}{1.45T_c}\right)-1.04}. \quad (2)$$

The value obtained from the calculation is equal to λ_{el-ph} = 0.48, suggesting that Zr_5Al_4 is a weakly coupled electron-phonon coupling superconductor. From the Sommerfeld coefficient and the electron-phonon coupling parameter the non-interacting density of states at the Fermi level DOS(E_F) can be estimated via the relation:

$$DOS(E_F) = \frac{3\gamma}{\pi^2 k_B^2 (1+\lambda_{el-ph})}, \quad (3)$$

where k_B is the Boltzmann constant. The thus determined $DOS(E_F)$ = 8.4 states per eV per formula unit (f.u.).

Fig. 4(b) shows the specific heat jump in the vicinity of superconducting transition temperature in different applied magnetic fields (0, 0.25 and 0.5 T). The vertical solid lines represent the midpoints of the transitions for each field and are used for calculation of the upper critical field (Fig. 5(b)). The size of the

superconducting anomaly becomes smaller and shifts towards lower temperature with increasing magnetic field.

The temperature dependence of electrical resistivity ρ(T) of Zr_5Al_4 is presented in the main panel of Fig. 5.

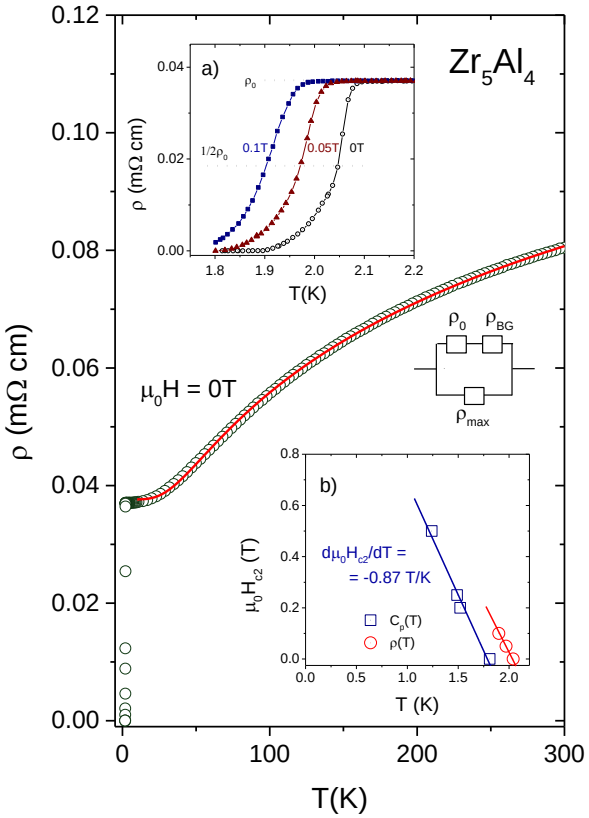

Fig. 5. Electrical resistivity of Zr_5Al_4. Main Panel: resistivity over a wide temperature range fitted with parallel resistor model, (a) Resistivity data near the superconducting transition in fields from 0 to 0.1 T, (b) Upper critical field as a function of temperature plotted with data from heat capacity (squares) and resistivity (circles) measurements.

Metallic behavior (dρ(T)/dT > 0) is manifested in the whole temperature range. Below 10 K the resistivity becomes temperature independent with a residual resistivity $\rho_r \sim 37$ μΩ cm. The residual resistivity ratio is rather low RRR = $\rho_{300}/\rho_r \approx 2$, which is common for polycrystalline samples [7,29,30]. The data above the superconducting transition was fitted with a parallel resistor model [31–33] in which Bloch-Grüneisen resistivity ρ_{BG} is combined with a parallel independent resistor ρ_{max}, as seen on the diagram in Fig. 5. In this model, the resistivity is described as:

$$\rho(T)^{-1} = \rho_P^{-1} + (\rho_0 + \rho_{BG})^{-1}, \quad (4)$$

where

$$\rho_{BG} = 4R\Theta\left(\frac{T}{\Theta}\right)^5 \int \frac{x^5}{(\exp(x)-1)(1-\exp(-x))}dx \quad (5)$$

The temperature independent resistivity ρ_0 estimated from the fit is 53 μΩ cm, saturation resistivity ρ_{max} = 127 μΩ cm and the characteristic temperature Θ = 202(1) K.

The results of resistivity ρ(T) measurements at low temperatures are shown in Fig. 5(b) to highlight the superconducting transition. The resistivity in zero-field drops below 2.1 K and reaches zero at 1.9 K. The transition temperature T_c = 2.04 K, determined as a midpoint of the resistivity drop, is higher than obtained from heat capacity and magnetic susceptibility measurements. This effect is likely caused by the surface superconductivity phenomena reported also in the Al containing samples [29,34]. The superconducting transition shifts to lower temperature with increasing magnetic field. These data (red circles), together with the data obtained from the specific heat measurement (blue squares), are shown in Fig. 5(b).

Table 1 Values of the normal and superconducting parameters of Zr_5Al_4 compared with ScV_2Al_{20} [7], $VAl_{10.1}$ [29,38] and $ReGa_5$ [1]. The T_c for Zr_5Al_4 was estimated from the specific heat measurement. *dirty limit, **clean limit.

parameter	**Zr_5Al_4 [this work]**	**ScV_2Al_{20}** [7]	**$VAl_{10.1}$** [29,38]	**$ReGa_5$** [1]
T_c (K)	1.82	1.00	1.53	2.1
γ (mJ mol^{-1} K^{-2})	29.4(2)	29.6	17.3	4.7
(mJ mol-at.$^{-1}$ K^{-2})	3.3	1.3	1.56	0.8
Θ_D (K)	347	536	341	314
$\Delta C_{el}/\gamma T_c$	1.41	1.46	1.42	1.6
$\lambda_{el\text{-}ph}$	0.48	0.41	0.42 / 0.51	0.51
$DOS(E_F)$ (eV^{-1} per f.u.)	8.4	9.00	5.2 / 4.9	1.3
$H_{c2}(0)$ (T)	1.09* 1.16**	0.333(4)	0.1	-
ξ_{GL} (Å)	173	314	800	-

The upper critical field of single-band type-II BCS superconductor can be calculated using the Werthamer-Helfand-Hohenberg (WHH) expression [35,36]:

$$\mu_0 H_{c2}(0) = -AT_C \frac{d\mu_0 H_{c2}}{dT}\Big| T = T_C, \quad (6)$$

where A is the purity factor (0.693 for dirty and 0.73 for clean limit). The slope $\mu_0 \frac{dH_{c2}}{dT} = -0.87 \frac{T}{K}$ is almost identical for both - heat capacity and resistivity series. Taking T_c = 1.82 K we obtained the upper critical field $\mu_0 H_{c2}(0)$ = 1.09 T for dirty and $\mu_0 H_{c2}(0)$ = 1.16 T for

clean limit. For a type-II superconductor the superconducting coherence length can be estimated by using the Ginzburg-Landau formula [37] $H_{c2} = \Phi_0/2\pi\xi^2_{GL}$, where $\Phi_0 = h/2e$ is the flux quantum. Taking $\mu_0 H_{c2}(0) = 1.09$ T, the coherence length for Zr_5Al_4 is $\xi_{GL}(0) = 173$ nm. The normal and superconducting parameters for Zr_5Al_4 are listed in Table 2 and compared with the parameters reported for $VAl_{10.1}$ [29,38], ScV_2Al_{20} [7] and $ReGa_5$ [1].

To gain an intrinsic insight into superconductivity and the electronic states of Zr_5Al_4, the electronic density of states (DOS) and band structure of Zr_5Al_4 were calculated by DFT with and without spin-orbit coupling (SOC) included.

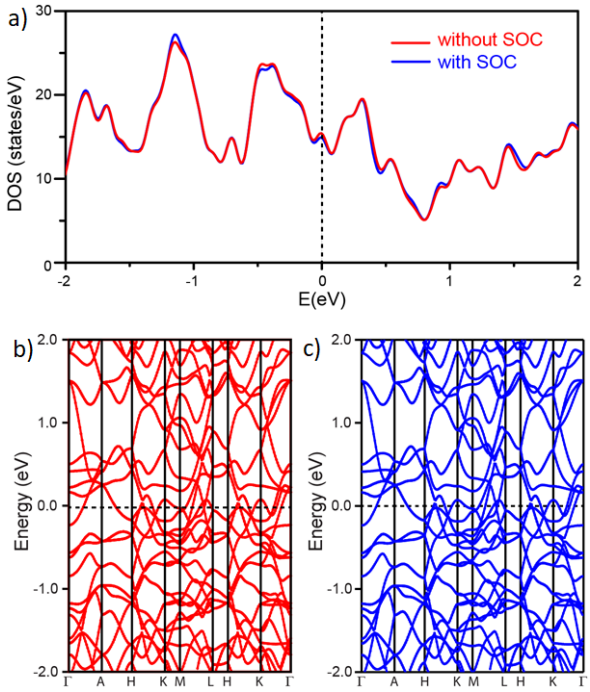

Fig. 6. (a) The total density of states (DOS) for Zr_5Al_4 with and without SOC. Bottom: The band structure (b) without and (c) with spin-orbit coupling for Zr_5Al_4

Fig. 6(a) illustrates the total density of states (DOS) for Zr_5Al_4 with and without SOC. The DOS in the energy below −2.0 eV is contributed mainly from Zr and Al *s* and *d*-orbitals. The DOS in the energy range from −2.0 eV to +2.0 eV is primarily attributed to mixed Zr and Al *s*, *d*-, and *p*- orbitals, in particular around the Fermi level. The relatively sharp peak in the DOS of Zr_5Al_4 near E_F can be taken as an indication of a nearby structural, electronic, or magnetic instability such as superconductivity. To get further insight, we calculated the band structure without and with spin-orbit coupling, presented in Fig. 6(b) and (c), respectively. The band structure shows that the peak at the Fermi level in the DOS is due to the presence of saddle points in the electronic structure at the M and L points in the Brillouin zone. Saddle points near E_F have been proposed as important for yielding superconductivity in a variety of materials [39].

The DOS(E_F) from DFT calculations has a value of ~ 15 states per eV per formula unit, which is almost two times higher than value calculated from the Sommerfeld coefficient and the electron-phonon coupling parameter (8.4 states per eV per formula unit). Using the value obtained from the electronic structure calculations, we can estimate the value of electronic heat capacity coefficient $\gamma_{calc} = \frac{\pi^2}{3} k_B^2 N(E_F) = 35.5$ mJ mol^{-1} K^{-2}, which is again higher than the experimental value: $\gamma_{exp} = 29.4$ mJ mol^{-1} K^{-2}.

IV Conclusions

We have successfully synthesized a polycrystalline sample of the high-temperature Zr_5Al_4 phase. Powder X-ray diffraction confirms the phase purity and the hexagonal structure in space group $P6_3/mcm$, with lattice parameters $a = 8.4312(6)$ Å and $c = 5.7752(8)$ Å. From magnetic susceptibility, heat capacity and resistivity measurements the material is found to be a type-II superconductor with the transition temperature $T_c = 1.82$ K. Analysis of the heat capacity data allowed us to estimate the electron-phonon coupling parameter $\lambda_{el-ph} = 0.48$, classifying Zr_5Al_4 as a weakly coupled superconductor. Comparison of the superconducting parameters for Zr_5Al_4 with Al-based ($Val_{10.1}$ and ScV_2Al_{20}) and Ga-based ($ReGa_5$) endohedral superconductors, all of which have a similar critical temperature reveals that all are weakly coupled superconductors with $\lambda_{el-ph} \sim 0.5$. The different Debye temperatures observed reflect different concentrations of the light Al atoms ($Val_{10.1}$ and ScV_2Al_{20}) or the presence of a heavier atom e.g. in $ReGa_5$. Interestingly, the Sommerfeld coefficient (calculated per mol-at.) is the largest for Zr_5Al_4.

Acknowledgements

The research performed at the Gdansk University of Technology was supported by the National Science Centre (Poland) grant (UMO-2016/22/M/ST5/00435). The work at LSU was supported by a Beckman Young Investigator Award. The work at Princeton was supported by the US Department of Energy, Division of Basic Energy Sciences, grant DE-FG02-98ER45706. MJW was supported by the Foundation for Polish Science (FNP).

References

[1] W. Xie et al., *Proc. Natl. Acad. Sci.* **112** (2015) E7048–E7054.
[2] P. Neha et al., *Mater. Res. Express.* **6** (2019) 016002.
[3] P. Neha et al., *AIP Conf. Proc.* **1832** (2017) 130048.
[4] V.Y. Verchenko et al., *Phys. Rev. B.* **96** (2017) 134504.
[5] J. Zhou et al., *Appl. Phys. Lett.* **108** (2016) 253102.
[6] W. Xie et al., *Inorg. Chem.* **55** (2016) 3203–3205.
[7] M.J. Winiarski et al., *Phys. Rev. B.* **93** (2016) 134507.
[8] M. Tsujimoto et al., *Phys. Rev. Lett.* **113** (2014) 267001.
[9] K. Matsubayashi et al., *Phys. Rev. Lett.* **109** (2012) 187004.
[10] A. Yamada et al., *J. Phys. Soc. Jpn.* **87** (2018) 033707.
[11] E.J. Little and M.M. Jones., *J. Chem. Educ.* **37** (1960) 231.
[12] R.V. Nandedkar et al., *Phys. Status Solidi A*. **73** (1982) K157–K160.
[13] T.J. Renouf and C.A. Beevers, *Acta Crystallogr.* **14** (1961) 469–472.
[14] T.J. Renouf, *Acta Crystallogr.* **15** (1962) 282–283.
[15] M. Alatalo et al., *Phys. Rev. B.* **57** (1998) R2009–R2012.
[16] K. Persson, Materials Data on Zr_5Al_4 (SG:193) by Materials Project, (2016).
[17] G.S. Pawley, *J. Appl. Crystallogr.* **14** (1981) 357–361.
[18] A.A. Coelho, TOPAS Academic: General Profile and Structure Analysis Software for Powder Diffraction Data, Bruker AXS, Karlsruhe, Germany, 2007.
[19] A. Jain et al., *APL Mater.* **1** (2013) 011002.
[20] K. Persson, Materials Data on Zr_4Al_3 (SG:191) by Materials Project, (2014).
[21] K. Persson, Materials Data on Zr_2Al_3 (SG:43) by Materials Project, (2015).
[22] T. Klimczuk and R.J. Cava, *Phys. Rev. B.* **70** (2004) 212514.
[23] Charles Kittel, *Introduction to Solid State Physics*, 8th Edition, NJ Wiley, Hoboken, 2004.
[24] A. Tari, *The specific heat of matter at low temperatures.*, Imperial College Press, London, 2003.
[25] L.C. Srivichitranond et al., *Phys. Rev. B.* **95** (2017) 174521.
[26] V.Y. Verchenko et al., *Phys. Rev. B.* **93** (2016) 064501.
[27] D. Singh et al., *Phys. Rev. B.* **94** (2016) 054515.
[28] W.L. McMillan, *Phys. Rev.* **167** (1968) 331–344.
[29] T. Klimczuk et al., *J. Phys. Condens. Matter.* **24** (2012) 365701.
[30] T. Klimczuk et al., *Phys. Rev. B.* **85** (2012) 174505.
[31] H. Wiesmann et al., *Phys. Rev. Lett.* **38** (1977) 782–785.
[32] C.H. Wang et al., *Phys. Rev. B.* **82** (2010) 094406.
[33] T. Klimczuk et al., *Phys. Rev. B.* **84** (2011) 075152.
[34] R.W. Cohen et al., *Phys. Rev.* **168** (1968) 444–450.
[35] N.R. Werthamer et al., *Phys. Rev.* **147** (1966) 295–302.
[36] E. Helfand et al., *Phys. Rev.* **147** (1966) 288–294.
[37] M. Tinkham, *Introduction to Superconductivity*, Courier Corporation, New York, 1996.
[38] D.J. Safarik et al., *Phys. Rev. B*. **85** (2012) 014103.
[39] W. Xie et al., *Chem. Mater.* **27** (2015) 4511–4514.
[40] K. Momma and F. Izumi, *J. Appl. Crystallogr*. **44** (2011) 1272–1276.